

## ARTICLE OPEN

Dislocations interaction induced structural instability in intermetallic  $\text{Al}_2\text{Cu}$ Qing Zhou<sup>1,2</sup>, Jian Wang<sup>1,2</sup>, Amit Misra<sup>3</sup>, Ping Huang<sup>1</sup>, Fei Wang<sup>4</sup> and Kewei Xu<sup>1</sup>

Intermetallic precipitates are widely used to tailor mechanical properties of structural alloys but are often destabilized during plastic deformation. Using atomistic simulations, we elucidate structural instability mechanisms of intermetallic precipitates associated with dislocation motion in a model system of  $\text{Al}_2\text{Cu}$ . Interaction of non-coplanar  $\langle 001 \rangle$  dislocation dipoles during plastic deformation results in anomalous reactions—the creation of vacancies accompanied with climb and collective glide of  $\langle 001 \rangle$  dislocation associated with the dislocation core change and atomic shuffle—accounting for structural instability in intermetallic  $\text{Al}_2\text{Cu}$ . This process is profound with decreasing separation of non-coplanar dislocations and increasing temperature and is likely to be operative in other non-cubic intermetallic compounds as well.

*npj Computational Materials* (2017)3:24; doi:10.1038/s41524-017-0030-2

## INTRODUCTION

Precipitation-hardening mechanisms have been widely applied for the development of high strength and ductile metallic alloys.<sup>1</sup> Al-matrix structural alloys that contain Al-based intermetallic precipitates are potential candidates for structural applications at ambient and elevated temperatures because of their significantly lightweight, four times lower density as compared to steel.<sup>2–10</sup> Through refining the characteristic dimension and distribution of intermetallic precipitates, the ductility and strength of Al-matrix composites can be significantly improved at room temperature. A high volume fraction of nanoscale intermetallic reinforcements (precipitate or lamina) can be realized with the help of either rapid solidification with alloying additions (for example, the directional solidification of metal-intermetallic lamellar eutectics)<sup>2–7</sup> or severe plastic deformation (SPD) techniques.<sup>8–12</sup> However, SPD often leads to destabilization of intermetallic phase, such as the formation of non-equilibrium solid solutions,<sup>8, 9</sup> disordering<sup>10, 11</sup> or amorphization.<sup>12</sup> These defects may accelerate the de-alloying and/or failure of intermetallic compounds, for example, the selective dissolution of Al from  $\text{Al}_2\text{Cu}$  in acid environments.<sup>13</sup>

Structural instability of intermetallic phase during heavy plastic deformation has been partially ascribed to dislocations and defected interfaces created during straining.<sup>14–21</sup> Dislocations in intermetallic phases are preferably nucleated from phase boundaries because of interface ledges/steps and slip transmission from matrix into precipitates.<sup>15–18</sup> Dislocations crossing the precipitates may drag interstitial or vacancy atoms with them out of the precipitate.<sup>14–16, 19</sup> In situ straining experiments of Al– $\text{Al}_2\text{Cu}$  composites in a transmission electron microscope (TEM) have shown dislocations bypassing through  $\text{Al}_2\text{Cu}$  plate-shaped precipitates by shear at multiple locations along the interphase boundaries.<sup>14</sup> Moreover, dislocations have been demonstrated

experimentally to climb in intermetallic phase,<sup>20, 21</sup> and provide rapid diffusion channels and adiabatic heating of the samples during plastic deformation.<sup>22, 23</sup> Nevertheless, glide dislocations and their reactions and non-conservative motion of dislocations are presumed to be responsible for structural instability of intermetallic phase.

For Al–Cu alloys, a number of metastable and stable precipitates of different shapes and sizes have been reported as strengthening precipitates in precipitation-hardened metals.<sup>2–12</sup> Intermetallic  $\theta$ - $\text{Al}_2\text{Cu}$  precipitates are formed in plate-like structures, acting as strengthening units.<sup>24</sup> In lamellar eutectic Al–Cu composite,  $\text{Al}_2\text{Cu}$  phase adopts the tetragonal C16 structure. There has been an interest in understanding high-strength and high plastic deformability in fine-scale Al– $\text{Al}_2\text{Cu}$  eutectics synthesized via chill casting or laser rapid solidification where  $\text{Al}_2\text{Cu}$  adopt the tetragonal C16 structure.<sup>2–7</sup>  $\text{Al}_2\text{Cu}$  precipitates or laminae can plastically deform via dislocations at elevated temperatures ( $>300^\circ\text{C}$ ).<sup>25, 26</sup> The possible dislocations in  $\text{Al}_2\text{Cu}$  ( $\theta$ ) are directly related to its C16 body centered tetragonal structure. The major slip systems include  $\{110\}\langle 001 \rangle$ ,  $\{110\}1/2\langle 111 \rangle$ ,  $\{200\}\langle 001 \rangle$ , and  $\{112\}1/2\langle 111 \rangle$ .<sup>26</sup> The dislocation with Burgers vector  $[001]$  on plane (110) might have a wide core and be glissile corresponding to the large planar faults observed experimentally.<sup>27, 28</sup> Using molecular dynamics (MD) simulations with empirical potentials, we studied core structure of  $\langle 001 \rangle$  dislocation on (110) plane.<sup>29</sup> Disregistry analysis across the shear plane revealed that a  $[001]$  dislocation on (110) plane dissociates into two partials bonded by a planar-extended core with a separation  $>1.5$  nm (also see Figs. S1 and S2 in Supplementary Information). Each partial has Burgers vector of  $1/2[001]$ . MD simulations also demonstrated the easy gliding of a  $\langle 001 \rangle$  dislocation on plane (110) at room temperature. In situ heating experiments of two-phase alloys performed inside a TEM indicate that the motion of dislocations in structural alloys often

<sup>1</sup>State key Laboratory for Mechanical Behavior of Material, School of Materials Science and Engineering, Xi'an Jiaotong University, Xi'an 710049, People's Republic of China;

<sup>2</sup>Mechanical and Materials Engineering, University of Nebraska-Lincoln, Lincoln, NE 68588, USA; <sup>3</sup>Department of Materials Science and Engineering, University of Michigan, Ann Arbor, MI 48109, USA and <sup>4</sup>State Key Laboratory for Strength and Vibration of Mechanical Structures, School of Aerospace, Xi'an Jiaotong University, Xi'an 710049, People's Republic of China

Correspondence: Jian Wang (jianwang@unl.edu) or Ping Huang (huangping@mail.xjtu.edu.cn) or Fei Wang (wangfei@mail.xjtu.edu.cn)

Received: 23 March 2017 Revised: 2 June 2017 Accepted: 16 June 2017

Published online: 04 July 2017

involves climb besides glide<sup>20, 21</sup> associated with change in their cores. It is questionable whether the planar extended core  $\langle 001 \rangle$  dislocation can climb, as the climb requires a very compact core structure for the dislocation.<sup>22</sup>

In this work, we investigated interaction of non-coplanar dislocation dipoles that mimic general cases of dislocations in a confined volume (precipitate or lamina), where dislocations are nucleated at the adjacent interfaces and glide toward each other. We unveiled that the planar-extended dislocation climbs at room temperature accompanying the creation of vacancies. This could account for structural instability of intermetallic compounds during mechanical deformation.

## RESULTS

### Climb of the planar-extended $\langle 001 \rangle$ dislocation

MD simulations demonstrated easy gliding of a  $\langle 001 \rangle$  dislocation on (110) plane glides at room temperature due to its wide planar-extended core (Movie 1 in Supplementary Information). Considering the fact of dislocations in a confined volume (precipitate), coplanar and non-coplanar dislocation dipoles form and interact. When non-coplanar dislocation dipoles move toward each other, the repulsive interaction force occurs in the certain range of distances,<sup>22, 30, 31</sup> and might enable collapse of the planar-extended core of the dislocation, in turn, probably favoring dislocation climb. We examined this idea by simulating reaction process of dislocation dipoles with various separation distances.

Figure 1 shows the simulation model that contains two full dislocations with opposite signed Burgers vector. A full dislocation with the Burgers vector  $[001]$  is dissociated into two partials (marked as 1 and 2) with the same Burgers vector  $\frac{1}{2}[001]$  that are positioned at the left of the simulation cell ( $x = -13.2$  nm), and another full dislocation with the Burgers vector  $[00\bar{1}]$  is dissociated into two partials (marked as 3 and 4) with the same Burgers vector  $\frac{1}{2}[00\bar{1}]$  that are positioned at the right of the simulation cell ( $x = 13.2$  nm). They are initially separated from a distance of 26.4 nm in the  $x$ -direction and a distance of  $h$  nm in the  $y$ -direction. Simulation models adopt the coordinates, the  $x$ -axis along  $[001]$ , the  $y$ -axis along  $[110]$ , and the  $z$ -axis along  $[\bar{1}\bar{1}0]$ , and have dimensions, 52 nm in the  $x$  direction, 30 nm in the  $y$  direction, and 1.71 nm in the  $z$  direction. The periodic boundary condition is applied along the  $x$ -axis and  $z$ -axis. The semi-fixed region is 1.5 nm from the top and bottom surfaces in the  $y$ -axis. During MD simulation, the temperature is set up at  $T = 300$  K and is controlled by applying the Langevin force to atoms. The nominal position of the two dislocations at each moment is

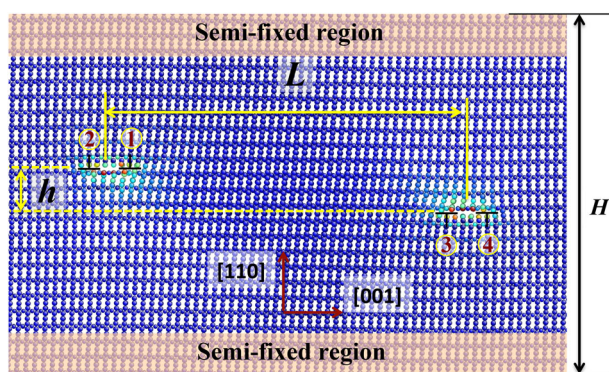


**Fig. 1** a Simulation set-up—two full dislocations are separated about  $L = 26.4$  nm along the horizontal direction and  $h$  nm along the vertical direction. The semi-fixed regions, 1.5 nm from the surfaces, retain applied shear strain and mimic bulk properties of Al<sub>2</sub>Cu. Atoms are colored according to their excess energy. The symbol “ $\perp$ ” indicates the position of dislocation

determined by the disregistry analysis.<sup>32</sup> We accelerate the dislocations by homogeneously straining the entire simulation model with a constant shear strain rate  $\dot{\gamma}_{yx} = 2 \times 10^8$ /s.

Figure 2a shows the simulation model that contains two full dislocations with opposite signed Burgers vector. The non-coplanar dislocation dipoles are separated for  $h = 2.83$  nm, corresponding to 27 atomic planes. During MD simulation at  $T = 300$  K, the intriguing finding is dislocation climb that is accompanied with the creation of vacancies. As the separation  $L$  is about 3 nm (corresponding to straining for 92 ps), Fig. 2b shows the climb of partial dislocation 3 upwards for four atomic planes, and the climb of partial dislocation 1 downwards for four atomic planes. After the climb, the two partials 1 and 2 (separated for four atomic planes) glide toward the right together; the two partials 3 and 4 (separated for four atomic planes) glide toward the left together. After straining for 132 ps, Fig. 2c shows the climb of partial 3 for total seven atomic planes from the initial glide plane. The partial 1 glides toward the right, extending the stacking fault because the partial 2 is pinned by vacancies. After straining for 172 ps, Fig. 2d shows that partial 3 climb for total eight atomic

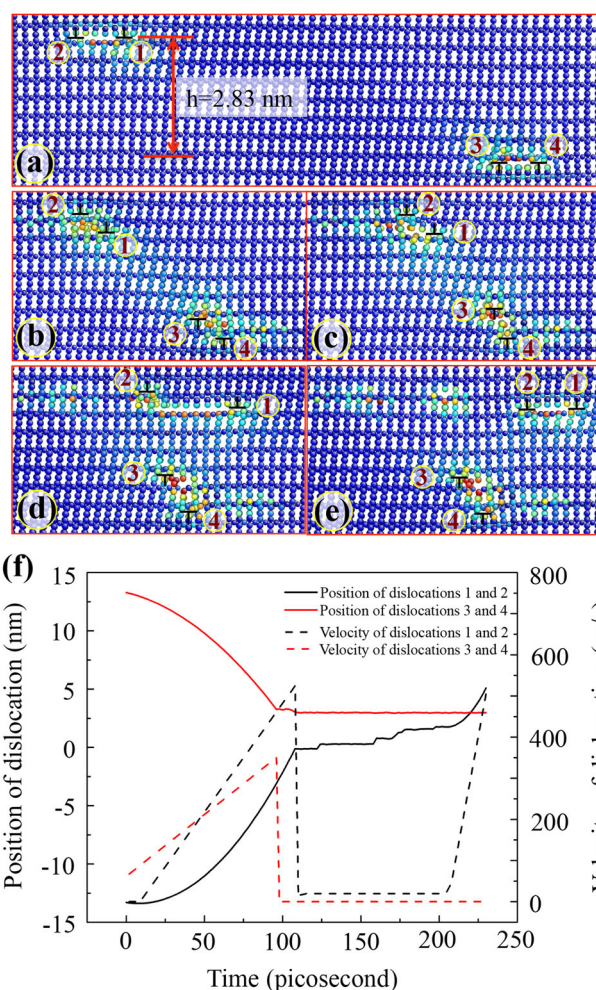


**Fig. 2** Interaction of a pair of dislocation dipole with the separation of  $h = 2.83$  nm. At temperature of 300 K, atomic structures associated with a the glide of four partials, b the climb of partials 1 and 3 for four atomic planes, c the climb of partial 3 for seven atomic planes, d the stacking fault is created associated with the glide of partial 1 and the pinning of partial 2, and the climb of partial 3 for eight atomic planes, and e the climb of partial 2 on the same plane as partial 1, and then they glide together. Dislocations annihilation does not happen. The symbol “ $\perp$ ” indicates the position of dislocation

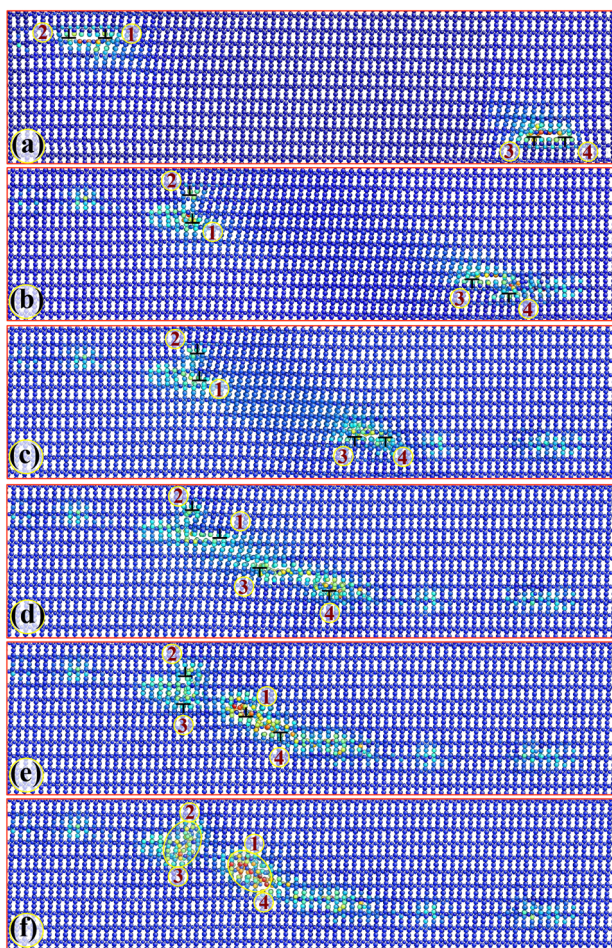


**Fig. 3** Interaction of a pair of dislocation dipole with the separation of  $h = 2.83$  nm. At temperature of 700 K, atomic structures associated with **a** the glide of four partials, **b** the climb of partials 1 for eight atomic planes and partial 3 for four atomic planes, **c** partial 4 climbs for four atomic planes, and glides with partial 3 on the same plane, **d** partials 1 and 3 attract each other, quickly move towards each other, **e** partials 2 and 3 are vertically positioned, forming vacancy cluster, and **f** partials 1 and 4 are vertically positioned, forming vacancy cluster. The symbol “L” indicates the position of dislocation

planes and the stacking fault associated with the glide of partial 1 is extended. After 176 ps, partial 2 climbs for four atomic planes and glides on the same shear plane with partial 1 as a full dislocation together (Fig. 2e). As a result, dislocations annihilation did not occur (also see Movie II in Supplementary Information). Figure 2f shows the position and velocity of dislocations with simulation time. The first climb occurs at  $t = 92$  ps, the corresponding separation  $L$  is 3.04 nm, and the shear stress is 2.0 GPa. The two sets of dislocations glide at velocities of 505 m/s for the dislocations 1 and 2 and 380 m/s for the dislocations 3 and 4, being far lower than the shear wave speed of Al<sub>2</sub>Cu. After partial 3 climbs for eight atomic planes, dislocations 3 and 4 are pinned by the vertical-extended core and vacancies. Partial 1 and 2 continuously glide after partial 2 climbs on the same shear plane as partial 1 is.

As dislocation climb is thermally activated, we increased simulation temperature to  $T = 700$  K and re-simulated the case (see Movie III in Supplementary Information). The first climb event happens much earlier at  $t = 42$  ps and the separation  $L = 14$  nm. At  $t = 210$  ps, Fig. 3b shows the climb of partial 1 downwards for total eight atomic planes, forming a vertical-extended 8-layer

dislocation; and the climb of partial 3 upwards four atomic plane and the creation of stacking fault between partials 3 and 4. It is noticed that the vertical-extended 8-layer dislocation glide together without creating stacking faults. After straining for 220 ps, Fig. 3c shows that the vertical-extended 8-layer dislocation (consisting of partials 1 and 2) glides slowly while two partials 3 and 4 glide together on the same shear plane after partial 4 climbs upwards for four atomic planes. When the two sets of dislocations are close at the distance of 2.0 nm, partials 1 and 3 attract each other and quickly move (glide and climb) toward each other (Fig. 3d). Figure 3e shows that partials 2 and 3 with opposite Burgers vectors are vertically positioned with a separation of 11 atomic planes in the  $y$  direction, resulting formation of vacancy cluster. Partial 1 and 4 with opposite Burgers vectors also attract each other, annihilating each other associated with formation of vacancy cluster (Fig. 3f). Finally, four partials annihilate.

We further examined dislocation climb for non-coplanar dislocation dipoles with different separations:  $h = 0.12$  nm corresponding to one Al plane;  $h = 0.28$  nm corresponding to three atomic planes;  $h = 1.13$  nm corresponding to 11 atomic planes. At  $T = 300$  K, MD simulations demonstrated the climb of partials associated with the creation of vacancies and collective glide of two vertically positioned partials. When the dipole is separated by one Al plane, the first climb occurs at the distance  $L = 12$  nm. Finally, the four partials annihilate (see Fig. S3 and Movie IV in Supplementary Information). When the dipole is separated by  $h = 0.28$  nm, the first climb occurs at the distance  $L = 7.4$  nm, and finally the four partials annihilate (see Fig. S4 and Movie IV in Supplementary Information). When the separation is  $h = 1.13$  nm, the first climb occurs at the distance  $L = 3.70$  nm. The four partials annihilate associated with the creation of a vacancy cluster (see Fig. S6 in Supplementary Information). When the separation is  $h = 2.83$  nm, the first climb occurs at the distance  $L = 3.04$  nm. Partial 1 climb and glide together, but annihilation did not occur (Fig. 2e). As simulation temperature increases to  $T = 700$  K, the first climb happens much earlier at the distance  $L = 14$  nm and finally the four partials annihilate (Fig. 3f).

#### Core change and vacancy creation associated with dislocation climb

MD simulations so far demonstrated both climb and glide of a full  $\langle 001 \rangle$  dislocation with planar-extended core—one partial climbs associated with the creation of vacancies, changing the planar-extended core to a vertical-extended core; the vertical-extended full dislocation collectively glides without creating stacking faults associated with atomic shuffle. Figure 4 shows the formation of vertical extended core after one partial climbs for four atomic planes and the collective glide of the two partials. Accompanying the climb of one partial 3, vacancies are created in the dislocation core region and pin the two partials (Fig. 4b); under continuous shearing, the two partials de-pin from the environment of vacancies (Fig. 4c). The numbers of created vacancies correspond to the Burgers vector and climb distance. Figure 4e shows the created 18 vacancies (12 vacancies in Al planes and 6 vacancies in Cu plane, the length of the dislocation line is three units along the  $z$ -axis). After de-pinning, the two partials with a vertical-extended core (four atomic planes separation in the  $y$  direction) collectively glide together on the adjacent planes. Such collective gliding does not create stacking faults (Fig. 4d) in the sheared region, implying that the collective glide is associated with atomic shuffle.<sup>33–35</sup> Fig. S5 in Supplementary information shows the position and velocity of the two full dislocations, and the shear stress as a function of time. It shows that a planar-extended dislocation glides faster than the vertical-extended dislocation.

The climb of a partial dislocation is associated with the creation of vacancies.<sup>36, 37</sup> MD simulations indicate a high formation energy for single vacancy,  $\sim 2.45$  eV, as one Cu or Al atom is

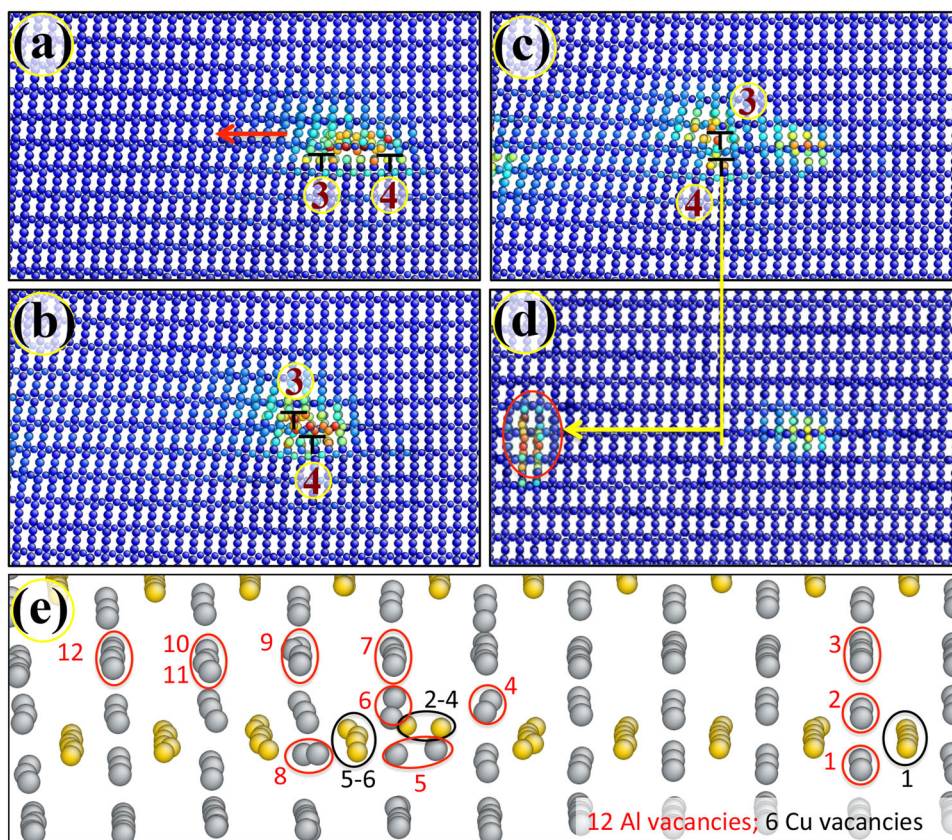


**Fig. 4** Four snapshots show atomic structure of a full dislocation during climb and collective glide. **a** One full dislocation dissociated into two partials 3 and 4; **b** One partial 3 climbs for four atomic planes associated with the creation of vacancies in dislocation core; **c** A vertical-extended dislocation with the vertical separation of four atomic plane; and **d** The vertical-extended dislocation de-pins from the environment of vacancies, and collectively glide for a distance of  $d$  without the creation of stacking fault. **e** Atomic structure shows the creation of 18 vacancies before the collective glide. Yellow atoms are Cu and gray atoms are Al. The circle indicates location of the  $i$ th vacancy. The symbol “L” indicates the position of dislocation

removed. Such high vacancy formation energy does not favor climb at room temperature. To address such a puzzle, we compared four defected configurations: the planar-extended dislocation, the vertical-extended dislocation (separated by four atomic planes), the vertical-extended dislocation surrounded by six vacancies (as the dislocation line is one unit long along  $\langle 110 \rangle$ ), and the vertical-extended dislocation away from six vacancies, as shown in Fig. 5a–d. We computed the excess energy of the defect region by integrating excess energy of atoms in a 9 nm cylinder with the axis at the center of two partials. The excess energy per unit length of  $\langle 110 \rangle$  is 34.61, 34.58, 36.70, and 40.58 (eV/d $_{\langle 110 \rangle}$ ), respectively. The planar-extended and vertical-extended dislocations have the same core energy, but they glide with different mechanisms. Most interestingly, the average formation energy of one vacancy is estimated to be 0.35 eV when these vacancies are surrounding the dislocation core, and 1.0 eV when they are closely distributed in a region away from the dislocation. This low formation energy of vacancy inside dislocation core is ascribed to nonlinearly strong interaction between vacancies and the dislocation core.<sup>22</sup>

MD simulations demonstrated that the vertical-extended full dislocation collectively glides without creating stacking faults. The crystallography of the projected atomic structure in Fig. 6a shows the atomic stacking of eight (110) planes in one unit cell: ... CuAl<sub>A</sub>Al<sub>B</sub>Al<sub>A</sub>CuAl<sub>C</sub>Al<sub>D</sub>Al<sub>C</sub>.... Two partials that are separated by four atomic planes (Al<sub>A</sub>CuAl<sub>C</sub>Al<sub>D</sub>) glide on two slip planes between Al<sub>B</sub>-Al<sub>A</sub> or Al<sub>D</sub>-Al<sub>C</sub>. Figure 6e is the plan-view of eight (110) planes in an unit cell, showing that the translation between Al<sub>A</sub> and Al<sub>C</sub> or

between Al<sub>B</sub> and Al<sub>D</sub> can be achieved through in-plane shear of  $\frac{1}{2}\langle 001 \rangle$ . When the two partials glide collectively without atomic shuffle, three Al planes of Al<sub>A</sub>CuAl<sub>C</sub>Al<sub>D</sub> between two shear planes are positioned at faulted sites Al<sub>C</sub>CuAl<sub>A</sub>Al<sub>B</sub> (Fig. 6b). Two possible shuffle mechanisms can correct the faulted region, as shown in Fig. 6c, d. The corresponding shuffle vectors are defined in Fig. 6a, e.  $e_1$  and  $e_2$  are equal to  $\pm 1/6[110]$ , corresponding to a magnitude of 0.14 nm.  $g_{s1}$  and  $g_{s2}$  are equal to  $\pm 1/6[110]$ , corresponding to a magnitude of 0.14 nm.  $s_1$  and  $s_2$  are equal to  $\pm 1/2[001]$ , corresponding to a magnitude of 0.24 nm. Atomistic simulations in Fig. 6f confirmed that the correction of Al<sub>B</sub> to Al<sub>D</sub> is accomplished through collective shuffle vectors ( $g_{s1}$  and  $g_{s2}$ ) on the atomic plane (110); but the correction of Al<sub>A</sub> and Al<sub>C</sub> is realized through vertical shuffle vectors ( $e_1$  and  $e_2$ ). The net shuffle displacements in one unit cell are equal to zero. This corresponds to the second mechanism (Fig. 6d). The same shuffle mechanism is also confirmed for collective glide of a vertically extended 8-layer dislocation (see Figs. S7 and S8 in Supplementary Information).

## DISCUSSION

The creation of vacancies accompanying dislocation climb could be responsible for structural instability of intermetallic precipitates. Dislocation motion has been identified experimentally to be one mechanism related to destabilization of intermetallic precipitates.<sup>11, 38–40</sup> For example, Jiao et al.<sup>38</sup> observed strain-induced precipitate dissolution in an irradiated austenitic alloy through

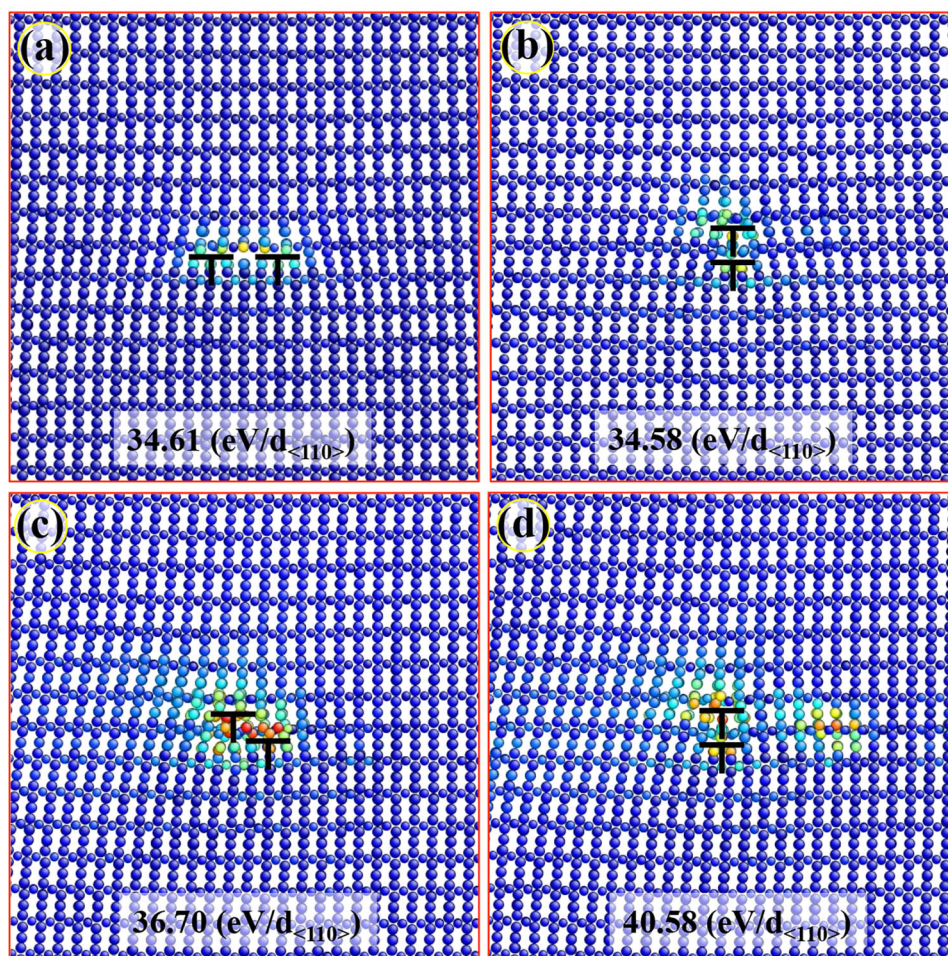


**Fig. 5** Atomic structures of two partials **a** with an extended planar core, **b** with a vertical core, **c** with a vertical core surrounded by six vacancies, and **d** with a vertical core and six vacancies away from the core. The symbol “ $\perp$ ” indicates the position of dislocation. The symbol “ $\perp$ ” indicates the position of dislocation

repetitive cutting by a large number of glissile dislocations; Murayama et al.<sup>40</sup> characterized the dissolution of precipitates in Al–Cu alloys after eight passes of equal channel angular pressing. Experimental studies also revealed the selective dissolution of Al from  $\theta$ -Al<sub>2</sub>Cu, and suggested that crystallographic defects, such as stacking faults and dislocations, facilitate de-alloying of  $\theta$ -Al<sub>2</sub>Cu.<sup>13, 41, 42</sup> The planar-extended and vertical-extended dislocation core could operate as precursor for de-alloying of  $\theta$ -Al<sub>2</sub>Cu because of the increased local stored energy. Moreover, dislocation climb driven by their interaction will create a high population of vacancies. Consequently, the high population of vacancies facilitates the diffusion of the alloying elements, thus accelerating de-alloying of Al from  $\theta$ -Al<sub>2</sub>Cu. In addition, it is conjectured that the easy climb of dislocations driven by dislocations interaction will reduce the glide ability of a dislocation, limiting plastic shear under mechanical loading.

The occurrence of dislocation climb driven by dislocation dipole interaction could generally occur in intermetallic compounds. Under mechanical loading, two dislocations (forming a dipole) are pushed close to each other. The interaction force (parallel to the glide plane) between two non-coplanar dislocations change from attraction to repulsion at a certain distance,<sup>22</sup> the repulsive force impedes the motion of the leading partial and consequently condenses the extended core. The interaction force (perpendicular to the glide plane) between two non-coplanar dislocations is always attractive, and facilitates dislocation climb by re-dissociating the condensed core into a vertical-extended core. Such a vertical-

extended core has the same core energy as the planar-extended core. In particular, the low formation energy associated with the creation of vacancies in the dislocation core region allows the occurrence of the climb. Such low formation energy of vacancies inside a dislocation core could be more profound in intermetallic compounds with non-cubic structures,<sup>43–45</sup> such as C16 body centered tetragonal structure (Al<sub>2</sub>Cu), D0<sub>22</sub> tetragonal structure (Al<sub>3</sub>Ti), D0<sub>20</sub> orthorhombic crystal structure (Al<sub>3</sub>Ni), and a monoclinic structure (Al<sub>3</sub>Fe) in which the slip plane is not closed packed and where a series of intermetallic compounds exist in the binary phase diagram. In contrast to Ni<sub>3</sub>Al, TiAl, FeAl, NiAl, and CoAl intermetallic compounds with cubic structures, their slip plane is closed packed with hexagonal atomic arrangement and the interaction of non-coplanar dislocation dipole in these compounds does not trigger dislocation climb (see Fig. S9 and Movie V in Supplementary Information).<sup>46</sup> Thus, the structural instability during plastic deformation identified in Al<sub>2</sub>Cu using MD simulations is likely to be operative in other intermetallic compounds and precipitates with non-cubic crystal structures where vacancies have relatively low formation energies inside non-compact dislocation core and glide plane are not closed packed.

## METHODS

Al<sub>2</sub>Cu ( $\theta$ ) is C16 body centered tetragonal structure. One unit cell contains 12 atoms with four Cu atoms and eight Al atoms. The lattice  $a = b = 0.606$  nm and  $c = 0.487$  nm. The crystal Al<sub>2</sub>Cu ( $\theta$ ) at room temperature has the

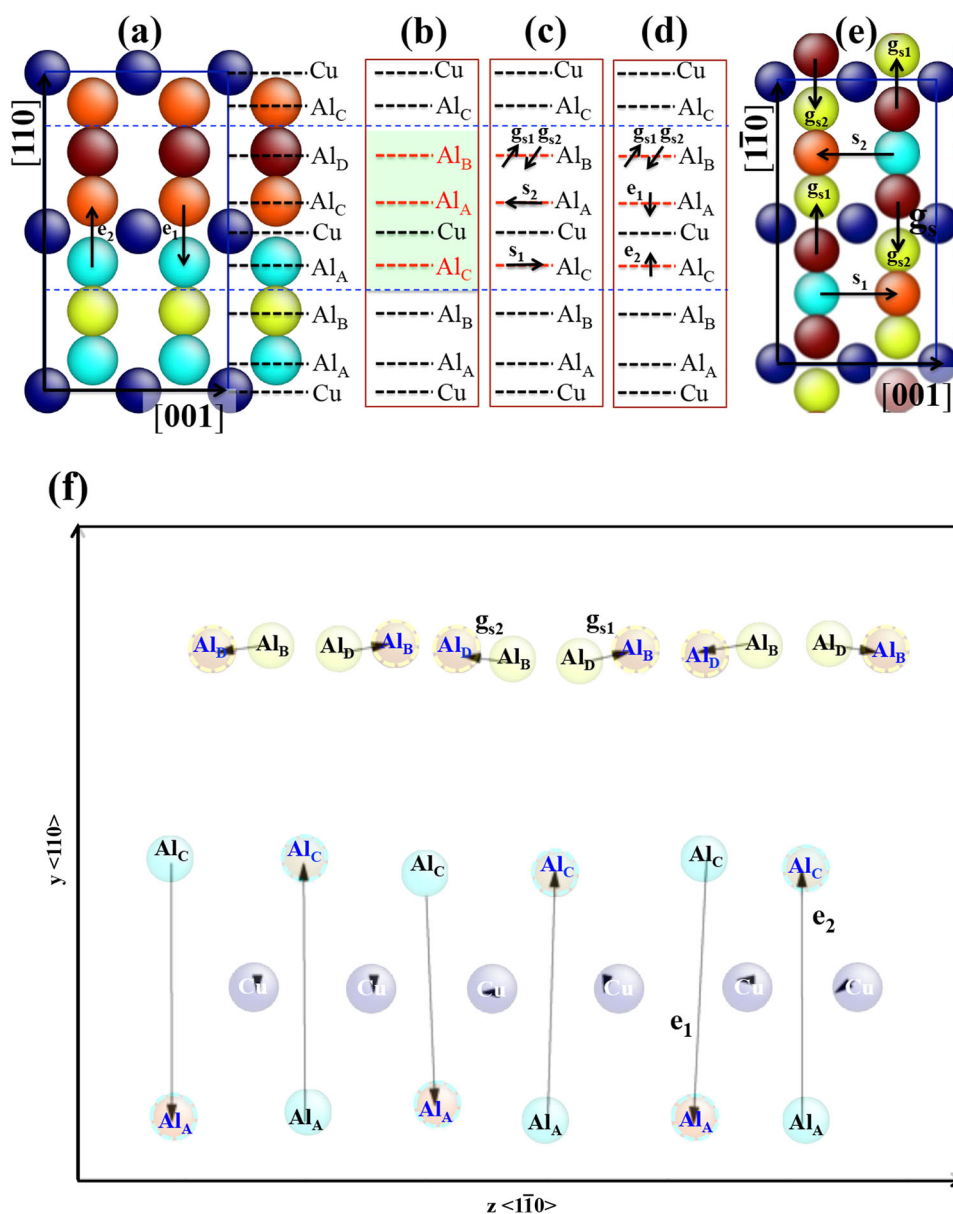


**Fig. 6** Collective glide of a vertical-extended dislocation with 4 atomic planes separation. The atomic structures of projection of a unit cell (a) along the  $\langle 10 \rangle$  direction, showing the atomic stacking of eight (110) planes in a unit cell: ...CuAIAIBAIAICuAICAIDAIC... and (e) along the  $\langle 110 \rangle$  direction, showing the plan-view of eight (110) planes. (b) The stacking change of four (110) atomic planes associated with collective gliding of two partials on the shear planes (blue dashed lines). (c) and (d) two possible shuffle mechanisms. The shuffle displacements are indicated in two projected planes (a) (1 0) and (e) (110). (f) Atomic displacements of atoms in one (001) plane, being consistent with shuffle mechanism in (d)

anisotropic elastic constants  $C_{11} = 159$  GPa,  $C_{12} = 63$  GPa,  $C_{13} = 49$  GPa,  $C_{33} = 163$  GPa,  $C_{44} = 29$  GPa,  $C_{66} = 46$  GPa.<sup>30</sup> Using atomistic simulations with empirical potentials, we studied core structure of dislocations associated with these slip systems.<sup>29</sup> The potentials have been tested to well reproduce lattice constants, cohesive energy, elastic properties, as compared to first-principles density function theory calculations and experiments.<sup>30, 31</sup> Additional calculation details specific to different separations are included in the Supplementary Information.

#### Data availability

The data sets generated during and/or analyzed during the current study are available from the corresponding author on reasonable request.

#### ACKNOWLEDGEMENTS

J.W. and A.M. acknowledge research sponsorship by DOE, Office of Basic Energy Sciences. P.H. acknowledge the National Natural Science Foundation of China (51171141 and 51471131), F.W. acknowledge the National Natural Science Foundation of China (51271141) and the Fundamental Research Funds for the Central Universities.

#### AUTHOR CONTRIBUTIONS

Q.Z. performed atomistic simulations and data analysis at University of Nebraska-Lincoln. J.W., Q.Z., F.W., and P.H. prepared the first draft of this manuscript and all authors participated the discussion and writing of this manuscript. J.W. and A.M. conceived this study.

## ADDITIONAL INFORMATION

**Supplementary Information** accompanies the paper on the *npj Computational Materials* website (doi:10.1038/s41524-017-0030-2).

**Competing interests:** The authors declare no competing financial interests.

**Publisher's note:** Springer Nature remains neutral with regard to jurisdictional claims in published maps and institutional affiliations.

## REFERENCES

- Umakshi, Y. in *Materials Science and Technology: A Comprehensive Treatment, Vol. 6, Plastic Deformation and Fracture of Materials* (eds Cahn, R. W., et al.) (VCH Publishers, 1993) Ch. 6, 251–310.
- Park, J. M. et al. High-strength bulk Al-based bimodal ultrafine eutectic composite with enhanced plasticity. *J. Mater. Res.* **24**, 2605–2609 (2009).
- Park, J. M. et al. Multi-phase Al-based ultrafine composite with multi-scale microstructure. *Intermetallics* **18**, 1829–1833 (2010).
- Witkin, D., Lee, Z., Rodriguez, R., Nutt, S. & Lavernia, E. Al–Mg alloy engineered with bimodal grain size for high strength and increased ductility. *Scr. Mater.* **49**, 297–302 (2003).
- Li, X., Ren, Z., Fautrelle, Y., Zhang, Y. & Esling, C. Morphological instabilities and alignment of lamellar eutectics during directional solidification under a strong magnetic field. *Acta Mater.* **58**, 1403–1417 (2010).
- Tiwary, C. S., Roy Mahapatra, D. & Chattopadhyay, K. Effect of length scale on mechanical properties of Al–Cu eutectic alloy. *Appl. Phys. Lett.* **101**, 171901 (2012).
- Lee, S. W. et al. Micro-to-nano-scale deformation mechanisms of a bimodal ultrafine eutectic composite. *Sci. Rep.* **4**, 6500 (2014).
- Cabibbo, M. Partial dissolution of strengthening particles induced by equal channel angular pressing in an Al–Li–Cu alloy. *Mater. Charact.* **68**, 7–13 (2012).
- Murayama, M., Horita, Z. & Hono, K. Microstructure of two-phase Al–1.7at%Cu alloy deformed by equal-channel angular pressing. *Acta Mater.* **49**, 21–29 (2001).
- Korzniok, A. V. et al. Nanocrystalline structure and phase transformation of the intermetallic compound TiAl processed by severe plastic deformation. *Nanostruct. Mater.* **11**, 17–23 (1999).
- Senkov, O. N., Froes, F. H., Stolyarov, V. V., Valiev, R. Z. & Liu, J. Microstructure of Aluminum-Iron alloys subjected to severe plastic deformation. *Scr. Mater.* **38**, 1511–1516 (1998).
- Inoue, A. Amorphous, nanoquasicrystalline and nanocrystalline alloys in Al-based systems. *Prog. Mater. Sci.* **43**, 365–520 (1998).
- Zhang, X., Hashimoto, T., Lindsay, J. & Zhou, X. Investigation of the de-alloying behaviour of  $\theta$ -phase (Al<sub>2</sub>Cu) in AA2024-T351 aluminium alloy. *Corros. Sci.* **108**, 85–93 (2016).
- Liu, G. *Time-Resolved and Three-Dimensional Study of Dislocation-Particle Interactions in Aluminum and Copper Alloys* (University of Illinois at Urbana-Champaign, 2011).
- Bonnet, R. HRTEM observation of a <113> low angle tilt boundary in the Al–Al<sub>2</sub>Cu ( $\theta$ ) Eutectic composite. *Phys. Stat. Sol.(a)* **189**, 183–196 (2002).
- Nie, J. F. & Muddle, B. C. Comments on the “dislocation interaction with semi-coherent precipitates ( $w$  phase) in deformed Al–Cu–Mg–Ag alloy”. *Scr. Mater.* **42**, 409–413 (2000).
- Salehinia, I., Shao, S., Wang, J. & Zbib, H. M. Interface structure and the inception of plasticity in Nb/NbC nanolayered composites. *Acta Mater.* **86**, 331–340 (2015).
- Wang, J., Zhou, Q., Shao, S. & Misra, A. Strength and plasticity of nanolaminated materials. *Mater. Res. Lett.* **5**, 1–19 (2017).
- Gridnev, V. N. & Gavriluyk, V. G. Cementite decomposition in steel during plastic deformation. (Review). *Phys. Met. (USSR)* **4**, 531–551 (1982).
- Appel, F. Diffusion assisted dislocation climb in intermetallic gamma TiAl. *Mater. Sci. Eng. A* **317**, 115–127 (2001).
- Anton, D. L., Shah, D. M., Duhl, D. N. & Giamei, A. F. Selecting high-temperature structural intermetallic compounds: the engineering approach. *JOM* **41**, 12–17 (1989).
- Hirth, J. P. and Lothe, J. *Theory of Dislocations* (Krieger Publishing Company, 1982).
- Schroll, R., Vitek, V. & Gumbsch, P. Core properties and motion of dislocations in NiAl. *Acta Mater.* **46**, 903–918 (1998).

- Russell, K. C. & Ashby, M. F. Slip in aluminum crystals containing strong, plate-like particles. *Acta Metall.* **18**, 891–901 (1970).
- Chanda, T. & Murty, G. S. Plastic behaviour of CuAl<sub>2</sub>. *J. Mater. Sci.* **27**, 5931–5934 (1992).
- Ignat, M. & Durand, F. Deformation lines on Al<sub>2</sub>Cu single crystals after creep in compression. *Scr. Metall.* **10**, 623–626 (1976).
- Knowles, K. M. & Stobbs, W. M. The structure of {111} age-hardening precipitates in Al–Cu–Mg–Ag alloys. *Acta Crystall. Section B: Struct. Sci.* **44**, 207–227 (1988).
- Bonnet, R. & Loubradou, M. Crystalline defects in a BCT Al<sub>2</sub>Cu( $\theta$ ) single crystal obtained by unidirectional solidification along [001]. *Phys. Stat. Sol. (a)* **194**, 173–191 (2002).
- Zhou, Q. et al. Atomistic study of fundamental character and motion of dislocations in intermetallic Al<sub>2</sub>Cu. *Int. J. Plastic.* **87**, 100–113 (2016).
- Chu, H. J., Wang, J. & Beyerlein, I. J. Anomalous reactions of a superplastic coplanar dislocation dipole: bypass or twinning? *Scr. Mater.* **67**, 69–72 (2012).
- Wang, J., Woo, C. H. & Huang, H. Destabilization of dislocation dipole at high velocity. *Appl. Phys. Lett.* **79**, 3621–3623 (2001).
- Wang, J., Hoagland, R. G., Liu, X. Y. & Misra, A. The influence of interface shear strength on the glide dislocation–interface interactions. *Acta Mater.* **59**, 3164–3173 (2011).
- Chu, F. & Pope, D. P. Deformation twinning in intermetallic compounds—the dilemma of shears vs. shuffles. *Mater. Sci. Eng. A* **49**, 39–47 (1993).
- Hirth, J. P., Wang, J. & Tomé, C. N. Disconnections and other defects associated with twin interfaces. *Prog. Mater. Sci.* **83**, 417–471 (2016).
- Wang, J. et al. Pure-shuffle nucleation of deformation twins in hexagonal-close-packed metals. *Mater. Res. Lett.* **1**, 126–132 (2013).
- Wang, J., Hoagland, R. G. & Misra, A. Room-temperature dislocation climb in metallic interfaces. *Appl. Phys. Lett.* **94**, 131910 (2009).
- Li, N., Wang, J., Huang, J. Y., Misra, A. & Zhang, X. In situ TEM observations of room temperature dislocation climb at interfaces in nanolayered Al/Nb composites. *Scripta Mater.* **63**, 363–366 (2010).
- Jiao, Z., McMurtrey, M. D. & Was, G. S. Strain-induced precipitate dissolution in an irradiated austenitic alloy. *Scr. Mater.* **65**, 159–162 (2011).
- Song, M. et al. Deformation-induced dissolution and growth of precipitates in an Al–Mg–Er alloy during high-cycle fatigue. *Acta Mater.* **81**, 409–419 (2014).
- Murayama, M. Z. & Hono, K. Microstructure of two-phase Al–1.7 at% Cu Alloy deformed by equal-channel angular pressing. *Acta Mater.* **49**, 21–29 (2001).
- Hashimoto, T. et al. Investigation of dealloying of  $\delta$  phase (Al<sub>2</sub>CuMg) in AA 2024-T3 aluminium alloy using high resolution 2D and 3D electron imaging. *Corros. Sci.* **103**, 157–164 (2016).
- Lebouil, S. et al. Dealloying of Al<sub>2</sub> Cu, Al<sub>7</sub>Cu<sub>2</sub>Fe, and Al<sub>2</sub>CuMg intermetallic phases to form nanoparticulate copper films. *Mater. Corros.* **65**, 416–424 (2014).
- Wolverton, C. Crystal structure and stability of complex precipitate phases in Al–Cu–Mg–(Si) and Al–Zn–Mg alloys. *Acta Mater.* **49**, 3129–3142 (2001).
- Yamagiwa, K. et al. Novel recycling system of aluminum and iron aastes-in-situ Al–Al<sub>3</sub>Fe functionally graded material manufactured by a centrifugal method. *Mater. Trans.* **44**, 2461–2467 (2003).
- Rajan, T. P. D., Pillai, R. M. & Pai, B. C. Functionally graded Al–Al<sub>3</sub>Ni in situ intermetallic composites: Fabrication and microstructural characterization. *J. Alloys Comp.* **453**, L4–L7 (2008).
- Purja Pun, G. P. & Mishin, Y. Development of an interatomic potential for the Ni–Al system. *Philos. Mag.* **89**, 3245–3267 (2009).



**Open Access** This article is licensed under a Creative Commons Attribution 4.0 International License, which permits use, sharing, adaptation, distribution and reproduction in any medium or format, as long as you give appropriate credit to the original author(s) and the source, provide a link to the Creative Commons license, and indicate if changes were made. The images or other third party material in this article are included in the article's Creative Commons license, unless indicated otherwise in a credit line to the material. If material is not included in the article's Creative Commons license and your intended use is not permitted by statutory regulation or exceeds the permitted use, you will need to obtain permission directly from the copyright holder. To view a copy of this license, visit <http://creativecommons.org/licenses/by/4.0/>.

© The Author(s) 2017